JOURNAL OF GEOPHYSICAL RESEARCH: OCEANS, VOL. 118, 6511–6524, doi:10.1002/2013JC009048, 2013

Arctic and Antarctic sea ice acts as a sink for atmospheric CO_2 during periods of snowmelt and surface flooding

Daiki Nomura,[1,2,3,4] Mats A. Granskog,[1] Philipp Assmy,[1] Daisuke Simizu,[2,4] and Gen Hashida[2]

Received 23 April 2013; revised 14 August 2013; accepted 8 October 2013; published 4 December 2013.

[1] In this study, we present evidence that Antarctic and Arctic sea ice act as sink for atmospheric CO_2 during periods of snowmelt and surface flooding. The CO_2 flux measured directly at the flooded sea ice surface (F_{flood}) constituted a net CO_2 sink of -1.1 ± 0.9 mmol C m^{-2} d^{-1} (mean $\pm$ 1 SD), which was an order of magnitude higher than the flux measured at the snow-air surface (F_{snow}) and bare ice surface (F_{ice}). The F_{snow}/F_{flood} ratio decreased with increasing water equivalent of snow and superimposed-ice, suggesting that the properties of snow and superimposed-ice formation affect the magnitude of the CO_2 flux. The F_{snow}/F_{flood} ratio ranged from 0.1 to 0.5, illustrating that 50–90% of the potential flux at the flooded surface was reduced due to the presence of snow/superimposed-ice. Hence, snow cover properties and superimposed-ice play an important role in the CO_2 fluxes across the sea ice-snow-atmosphere interface.

Citation: Nomura, D., M. A. Granskog, P. Assmy, D. Simizu, and G. Hashida (2013), Arctic and Antarctic sea ice acts as a sink for atmospheric CO_2 during periods of snowmelt and surface flooding, *J. Geophys. Res. Oceans*, *118*, 6511–6524, doi:10.1002/2013JC009048.

1. Introduction

[2] The ocean plays a crucial role in regulating atmospheric CO_2 through physical, chemical, and biological processes [*Takahashi et al*., 2009 and references therein]. Exchange of CO_2 occurs at the air-water interface. Hence, to understand the global carbon cycle, it is important to constrain the CO_2 sources and sinks in the world's oceans. So far, CO_2 flux studies have been largely restricted to open, ice-free areas of the ocean [*McNeil et al*., 2007]. This is mainly due to the fact that the presence of sea ice hampers ship-born observations. However, recent icebreaker cruises have added new data from ice covered seas [*Fransson et al*., 2011] and polynyas [*Else et al*., 2013]. Although effects of sea ice formation and melting on the carbon cycle of polar oceans have been highlighted [*Rysgaard et al*., 2011], processes related to the freezing and melting of sea ice still represent large unknowns to the exchange of CO_2 with the atmosphere [*Parmentier et al*., 2013].

[3] Although sea ice covers 12% of the world's ocean surface [*Comiso*, 2010], it has not been considered in estimates of the global carbon budget because of the assumption that sea ice impedes exchange of CO_2 with the atmosphere. Ice covered oceans were therefore not taken into account for the air-sea CO_2 flux in model [*Yager et al*., 1995; *Sun and Matsumoto*, 2010] and observational studies [*Bates*, 2006]. However, recent air-sea ice CO_2 flux measurements indicate that gas exchange of CO_2 occurs through sea ice [*Semiletov et al*., 2004; *Delille*, 2006; *Nomura et al*., 2006; *Zemmelink et al*., 2006; *Nomura et al*., 2010a, 2010b; *Loose et al*., 2009; *Miller et al*., 2011a; *Papakyriakou and Miller*, 2011; *Sejr et al*., 2011; *Geilfus et al*., 2012]. Although many unresolved issues remain, there seems little doubt that sea ice is permeable to CO_2 and other gases. Based on the limited data obtained from field observations in the Arctic, Antarctic, and Sea of Okhotsk as well as laboratory experiments conducted at different surface conditions and seasons (temperature) and with different methods [*Semiletov et al*., 2004; *Delille*, 2006; *Nomura et al*., 2006; *Zemmelink et al*., 2006; *Nomura et al*., 2010a, 2010b; *Loose et al*., 2009; *Miller et al*., 2011a; *Papakyriakou and Miller*, 2011; *Sejr et al*., 2011; *Geilfus et al*., 2012], one can conclude that the air-sea ice CO_2 flux depends on (i) the gradient of the partial pressure of CO_2 (pCO_2) between the sea ice surface and overlying air and (ii) sea ice surface conditions including the snow deposited on sea ice.

[4] Because the variation of pCO_2 in air is generally small compared to that in sea ice [*Delille*, 2006; *Miller et al*., 2011b], it is reasonable to assume that the air-sea ice CO_2 flux is driven by the pCO_2 at the sea ice surface. The pCO_2 in sea ice (brine) varies due to carbonate chemistry [*Delille et al*., 2007; *Fransson et al*., 2011], biological activity [*Delille et al*., 2007; *Thomas et al*., 2010], and $CaCO_3$ (ikaite) formation/dissolution [*Dieckmann et al*., 2008; *Papadimitriou et al*., 2012]. If brine pCO_2 is higher (lower) than that in the air, sea ice brine has the potential to release (absorb) CO_2 to (from) the atmosphere.

[5] Also the physical condition at the ice surface affects the magnitude of the air-sea ice CO_2 flux [*Delille*, 2006;

[1]Norwegian Polar Institute, Fram Centre, Tromsø, Norway.
[2]National Institute of Polar Research, Tachikawa, Japan.
[3]Japan Society for the Promotion of Science, Chiyoda, Japan.
[4]Institute of Low Temperature Science, Hokkaido University, Sapporo, Japan.

Corresponding author: D. Nomura, Institute of Low Temperature Science, Hokkaido University, Kita-19, Nishi-8, Kita-ku, Sapporo, Hokkaido 060-0819, Japan. (daiki@lowtem.hokudai.ac.jp)

2169-9275/13/10.1002/2013JC009048

Nomura et al., 2010a; *Miller et al*., 2011a; *Geilfus et al*., 2012]. For bare ice (no snow cover), the gas exchange occurs at the open brine channel-atmosphere interface [*Delille*, 2006; *Nomura et al*., 2006]. Brine volume fraction decreases with decreasing ice temperature [*Cox and Weeks*, 1983], and air-sea ice gas exchange is more or less inhibited at less than 5.0–7.5% brine volume fraction due to the reduction of permeability of sea ice [*Golden et al*., 1998; *Pringle et al*., 2009; *Zhou et al*., 2013]. Generally, air-sea ice CO_2 flux is at its minimum in the winter season due to low sea ice temperatures and consequently reduced permeability [*Delille*, 2006; *Miller et al*., 2011a; *Geilfus et al*., 2012].

[6] Snow on sea ice also affects the air-sea ice CO_2 flux [*Nomura et al*., 2010a; *Geilfus et al*., 2012]. *Nomura et al*. [2010a] showed that melting snow on sea ice (>9 cm) acts as physical barrier for CO_2 exchange between the air and sea ice even though the brine within the sea ice has the potential to exchange CO_2. However, studies that examined the air-soil CO_2 flux on snow covered soil [*Sommerfeld et al*., 1993, 1996; *Winston et al*., 1995; *Takagi et al*., 2005; *Elberling*, 2007; *Schindlbacher et al*., 2007; *Bowling and Massman*, 2011] have shown that the snow cover deposited over soils acts as a porous medium for CO_2. While CO_2 concentrations in soils drive the overall CO_2 flux through the snow cover, temporal and spatial variability of the CO_2 flux would be caused by specific snow properties [e.g., *Schindlbacher et al*., 2007]. Thus, snow properties over sea ice are also an important factor affecting the air-sea ice CO_2 flux. However, there is no study to date that has focused on the role of snow properties for the air-sea ice CO_2 flux. Snow properties (e.g., temperature, density, and salinity) do not only change on seasonal but also shorter time scales due to variations in air temperature and solar radiation that drive snow metamorphosis. Therefore, detailed measurements of snow properties are necessary to improve the assessments of the air-sea ice CO_2 flux.

[7] Another characteristics of the sea ice surface during heavy snow load or snowmelt is the formation of a slush layer [*Haas et al*., 2001; *Kattner et al*., 2004; *Ackley et al*., 2008; *Zemmelink et al*., 2006, 2008; *Papadimitriou et al*., 2009; *Nomura et al*., 2012, 2013]. High biological activity [*Kattner et al*., 2004] and meltwater supply from snow and ice surface melting [*Nomura et al*., 2012] alter the biogeochemical properties of the slush layer. The slush layer therefore has a strong effect on the air-sea ice CO_2 [*Zemmelink et al*., 2006] and dimethylsulfide (DMS) flux [*Zemmelink et al*., 2008; *Nomura et al*., 2012]. The exchange process through the slush layer would be promoted by active gas exchange at the slush-atmosphere interface compared to only partially open brine channels at the ice surface. It is important to note that the formation of slush layers likely occurs frequently during spring melt [*Haas et al*., 2001; *Kattner et al*., 2004; *Ackley et al*., 2008; *Zemmelink et al*., 2006, 2008; *Papadimitriou et al*., 2009; *Nomura et al*., 2012, 2013] and these processes may become more prevalent in the future.

[8] In this study, we examined the air-sea ice CO_2 flux over Antarctic multiyear land-fast ice in Lützow-Holm Bay, eastern Antarctica during the austral summer of 2010 and over Arctic first-year pack ice north of Svalbard in boreal spring 2011. For CO_2 flux measurements over sea ice, we developed a new system composed of three automatic open-close chambers with an integrated CO_2 measuring system, which allow us to evaluate the influence of different surface conditions at the same time as well as temporal variations in the air-sea ice CO_2 flux. The objectives of this study were to examine: (1) the effect of ice surface conditions (including snow properties) on the air-sea ice CO_2 flux and (2) the temporal variations in the air-sea ice CO_2 flux. Our results provide a useful baseline for future studies as the ongoing drastic changes in polar climate and sea ice extent are likely to alter the air-sea ice CO_2 flux in polar oceans.

2. Materials and Methods

2.1. Study Area

[9] The Antarctic study was part of the 51st Japanese Antarctic Research Expedition (JARE51) to the land-fast, multiyear sea ice station in Lützow-Holm Bay, Antarctica (68°56′–68°59′S, 38°57′–39°37′E) from January to February 2010 (Figure 1 and Table 1). Measurements and sampling were performed on 2, 5, 11, 18, and 19 January 2010 at the fixed ice stations (JARE51-M) near Syowa station and on 10 February 2010, about 30 km west of Syowa station (JARE51-S). The air temperature and the wind speed measured at Syowa station (Japan Meteorological Agency; http://www.data.jma.go.jp/obd/) during the observation period were $+0.4 \pm 1.8$°C (mean ± 1 SD) and 7.1 ± 6.1 m s^{-1}, respectively. The sea ice surface was flooded at all stations because the heavy snow load resulted in a negative freeboard (Table 1). In addition, freshwater supply from the melting snow and ice surface also contributed to the formation of a flooded surface slush layer (Table 1). Additionally, at the bottom of the snow cover, we observed superimposed-ice (an ice layer formed by the freezing of snow meltwater) (Table 1). Further details on site characteristics are described in *Nomura et al*. [2012].

[10] The Arctic study was performed during the Centre for Ice, Climate and Ecosystems cruise (ICE11) with R/V *Lance* to the pack ice north of Svalbard (80°47′–81°09′N, 12°26′–16°27′E) from April to May 2011 (Figure 1 and Table 1). Measurements and sampling were carried out on 29 and 30 April and 2, 3, 6, and 11 May 2011. During the observation period the air temperature and wind speed, measured at the mast of R/V *Lance*, were -5.5 ± 4.9°C and 6.8 ± 3.3 m s^{-1}, respectively. At some stations the sea ice was flooded but no superimposed-ice was observed (Table 1). Further details on site characteristics are described in *Nomura et al*. [2013].

2.2. Sea Ice CO_2 Flux Chamber Measurements

[11] The air-sea ice CO_2 flux was measured with a closed chamber approach, allowing direct determination of the in situ gas flux over sea ice [*Delille*, 2006; *Nomura et al*., 2010a, 2010b; *Geilfus et al*., 2012]. In this study, we used a new chamber system composed of three automatic open-close chambers and a gas analyzer (Figure 2), which allowed us to study the different surface conditions simultaneously as well as temporal variations of the air-sea ice CO_2 flux. This system was originally developed at Hokkaido University for soil CO_2 flux measurements. For operation on sea ice and snow, a collar with a serrated bottom

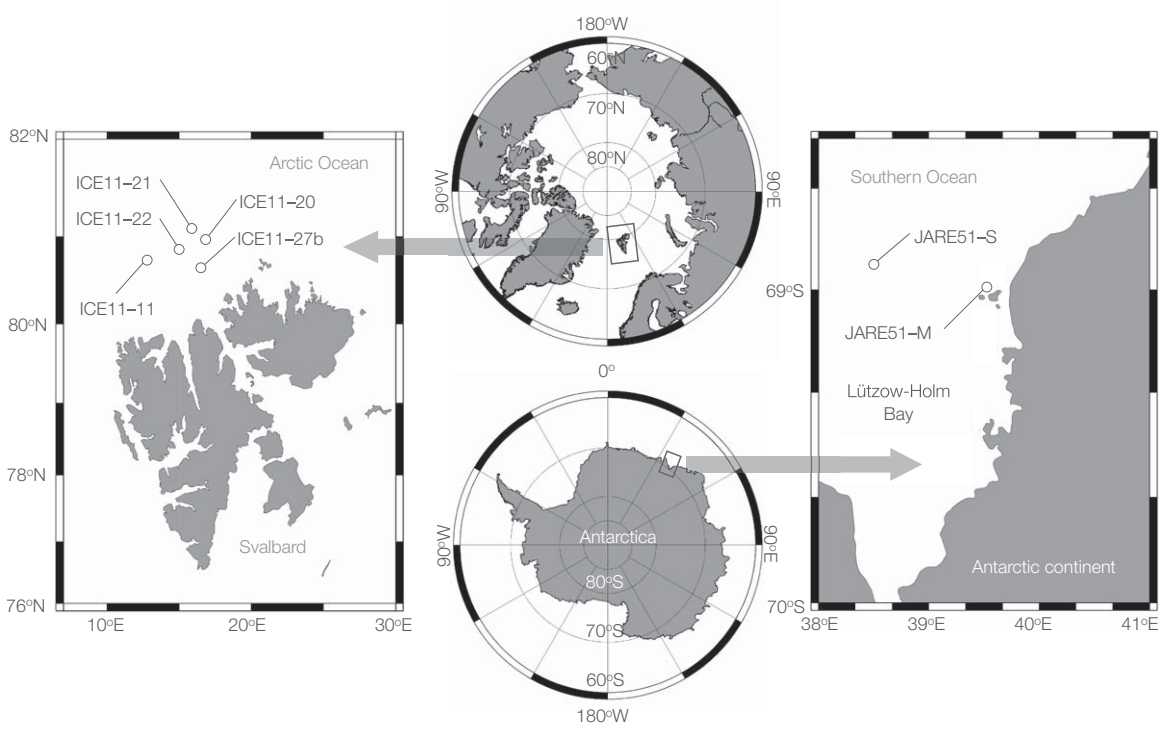

Figure 1. Location map of the sampling area for the Lützow-Holm Bay, Eastern Antarctica and north of Svalbard.

edge was developed (Figure 2b). Three chambers (each 40 cm in diameter and 12 cm in height) were made from a polyvinyl chloride pipe (Figure 2b). Temperature in the chamber was measured using a temperature data logger (RTR 52, T & D Corp., Nagano, Japan).

[12] A nondispersive infrared gas (NDIR) analyzer (Model 800, LI-COR Inc., Lincoln, NE, USA) was used for CO_2 concentration measurements (see Figure 2c). The NDIR analyzer and chambers were connected to a system controller (SC), including a data logger (Model 10x, Campbell Scientific Inc., Logan, UT, USA) that controls the opening/closing of the chambers. These devices were installed in a portable polypropylene box (62 × 38 × 33 cm). Electricity was supplied by a portable electric generator (Model EU16i, Honda Motor Co., Ltd, Tokyo, Japan) during JARE51 and a battery (Model 8012-254, Optima Batteries Inc., Milwaukee, WI, USA) during the ICE11 study. To avoid contamination by CO_2, the electric generator, used during JARE51, was installed at the downwind side more than 20 m away from the chambers. To calibrate the CO_2 measuring system before and after observations, four standards (mixing ratio of 324, 341, 363, and 406 ppm) traceable to the World Meteorological Organization (WMO) mole fraction scale [*Inoue and Ishii*, 2005] were used. Each CO_2 flux measurement was generally carried out from morning to afternoon. For the temporal study on

Table 1. Station, Date for CO_2 Flux Measurement and Sampling, Position, Air Temperature, Wind Speed, and Thickness of Snow, Superimposed-Ice, Flooded Slush Layer, and Sea Ice

Station	Date	Position	Air Temperature (°C)[a]	Wind Speed (m s^{-1})[a]	Thickness			
					Snow	Superimposed-Ice	Slush Layer	Sea Ice
JARE51-M	2 Jan 2010	68°59′44″S, 39°37′24″E	−0.2	10.8	30.0	13.0	17.0	188.0
JARE51-M	5 Jan 2010	68°59′44″S, 39°37′24″E	+1.7	2.9	34.0	11.0	14.0	157.0
JARE51-M	11 Jan 2010	68°59′44″S, 39°37′24″E	+2.9	2.5	30.0	9.0	38.0	155.0
JARE51-M	18 and 19 Jan 2010[b]	68°59′44″S, 39°37′24″E	+1.4	1.5	9.0	6.0	11.0	152.0
JARE51-S	10 Feb 2010	68°56′21″S, 38°57′08″E	+1.2	4.0	68.0	15.0	30.0	430.0
ICE11-11	29 and 30 Apr 2011[c]	80°47′38″N, 12°26′05″E	−0.9	6.5	15.0	0.0	6.0	88.0
ICE11–20	2 May 2011	81°03′09″N, 16°27′00″E	−0.1	2.1	19.6	0.0	7.0	58.0
ICE11–21	3 May 2011	81°09′43″N, 16°02′41″E	−8.3	8.5	25.0	0.0	0.0	125.0
ICE11–22	6 May 2011	80°55′47″N, 15°16′44″E	−1.2	8.5	30.0	0.0	0.0	119.0
ICE11–27b	11 May 2011	80°48′01″N, 16°17′27″E	−10.3	3.0	1.0	0.0	10.0	31.0

[a]Mean value during the period of CO_2 flux measurements.
[b]Sea ice coring was conducted on 19 January 2010.
[c]Sea ice coring and CO_2 flux measurements were performed on 29 and 30 April 2011, respectively.

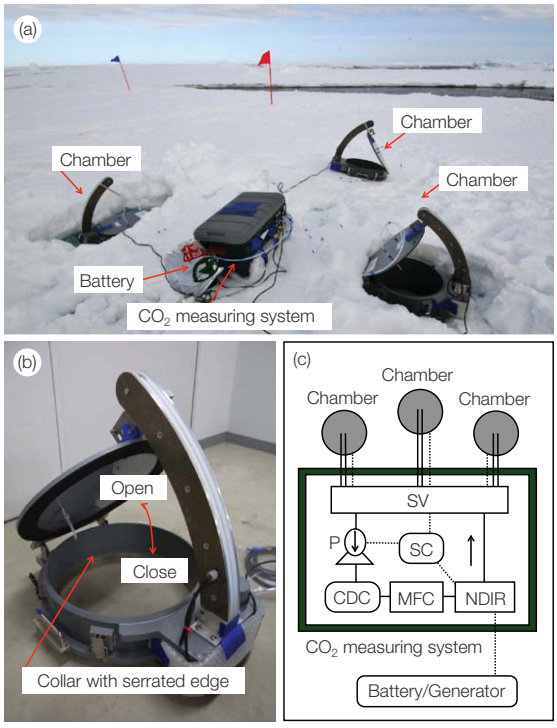

Figure 2. (a) Photographs of the CO_2 flux chamber system at station ICE11-11 north of Svalbard on 30 April 2011 and (b) scaled close up of one of the chambers. (c) Schematic diagram of the CO_2 flux chamber system. Sample air from the chambers was passed at a flow rate of 1.0 L min^{-1} by a diaphragm pump (P) through 1/4 in. Teflon tubes connected to a nondispersive infrared gas (NDIR) analyzer, a chemical desiccant column of $Mg(ClO_4)_2$ (CDC), solenoid valves (SV), and a mass flow controller (MFC). Solid and dashed lines indicate the closed loop of flowing air for measuring the air CO_2 concentration in the chambers and the electric circuit, respectively.

Antarctic sea ice (JARE51-M), the chambers were installed over an undisturbed area of approximately 25 m^2 and brought back to the lab after each day, except for continuous measurements on 18 and 19 January 2010. To examine the CO_2 flux under different surface conditions, we performed simultaneous chamber measurements within an area of 4 m^2 under three different surfaces (e.g., Figure 2a). Generally, chambers were installed over undisturbed snow, ice surface (superimposed-ice and sea ice), and flooded slush surface, the latter two after removing the snow and superimposed-ice (see below).

2.3. CO_2 Flux Measurements Over the Snow Surface (F_{snow})

[13] Snow surface CO_2 flux (F_{snow}) measures CO_2 flux at the snow-atmosphere interface. First, a collar with a serrated bottom edge was inserted 3 cm into the snow 30–60 min before measurements in order to avoid the disturbance by installation. Then, the measuring chamber was placed on top of the preinstalled collar.

2.4. CO_2 Flux Measurement on Bare Ice Surface (F_{ice})

[14] CO_2 flux measurements over the ice (F_{ice}) were similar to measurement of F_{snow}, except that the chamber was placed directly over the ice surface. Within 2 m of the F_{snow} chamber, approximately 1 m^2 of snow was removed by a snow shovel. A collar with a serrated bottom edge was inserted 3 cm into the ice surface 30–60 min before the chamber was placed on top of the preinstalled collar, and only then measurements were started. After removing the snow, surface conditions were representative of superimposed-ice for the Antarctic ice stations and nonflooded ice (bare ice) for the Arctic ice stations ICE11–21 and 22 (Table 1). Measurements of F_{ice} over superimposed-ice were examined at JARE51-M on 5 January 2010 and at JARE51-S on 10 February 2010.

2.5. Flooded Slush Surface CO_2 Flux (F_{flood})

[15] CO_2 flux measurements over the flooded slush layer (F_{flood}) were similar to measurement of F_{snow}, except that the chamber was placed directly over the slush after the overlying snow or superimposed-ice had been carefully removed without disturbing the slush layer. This chamber was within 2 m of the two other chambers. After snow and superimposed-ice removal, ice crystals in the flooded slush layer were removed with a net. A 15 cm high collar was inserted into the slush layer 30–60 min before measurements started.

2.6. CO_2 Flux Calculation

[16] Each of the three chambers were closed in sequence for 20 min, with the two other open, and in the closed chamber the CO_2 concentration was measured every 5 s. Thus in 1 h, one 20 min measurement period was performed for each chamber. As an example, the CO_2 concentration over the snow (F_{snow}), superimposed-ice (F_{ice}), and flooded slush layer (F_{flood}) at JARE51-M on 5 January 2010 is shown in Figure 3. The air CO_2 concentration in the chamber decreased with time (e.g., F_{flood}), indicating that CO_2 was absorbed from air to the slush surface. The CO_2 flux was calculated according to:

$$F = \rho(273.15/T)(dC/dt)(V/A) \quad (1)$$

where F is the flux (mmol C m^{-2} d^{-1}) (negative value indicates CO_2 being absorbed from air to ice surface), ρ the CO_2 density at standard temperature and pressure (=44.5 mol m^{-3} × (12/44)), T the temperature in the chamber (°K), dC/dt the rate of time variation (ppm d^{-1}) of CO_2 concentration in chamber (e.g., slope of Figure 3b), V the volume (m^3) of the chamber headspace adjusted for the volume occupied by the solid phase, and A the surface area (m^2) covered by the chamber. The values of 12 and 44 indicate the atomic mass of carbon and molecular mass of CO_2, respectively. The ratio of 273.15/T corrects for the temperature effect relative to the standard state. The stability of our NDIR sensor has been verified during CO_2 concentration measurements. The standard error of the regression line between the CO_2 concentration and elapsed time was <0.1 ppm (Figure 3b). The precision of CO_2 flux measurements based on the repetitive measurements ($n = 5$) within the same time frame (1–2 h) and at the same surface condition, was ±7%. The uncertainty of the CO_2 flux measurements, estimated from the standard error of the regression line between the CO_2 concentration and elapsed time was ±0.1 mmol C m^{-2} d^{-1}.

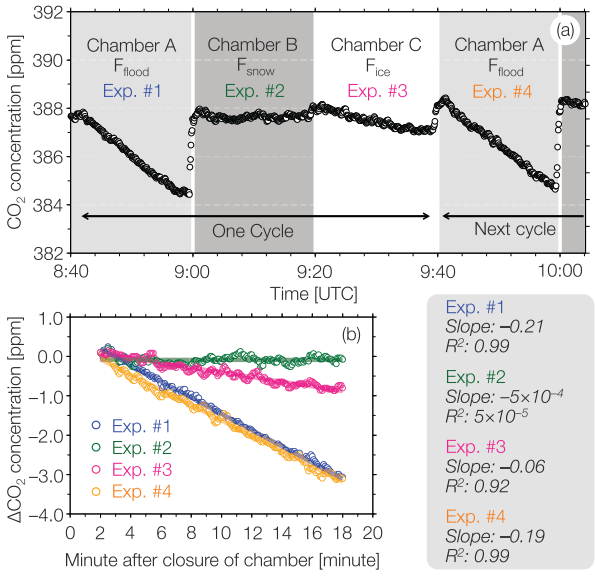

Figure 3. (a) Example of the temporal variation in CO_2 concentration in the chambers installed over the slush (Chamber A, Exps. 1 and 4), snow (Chamber B, Exp. 2), and superimposed-ice (Chamber C, Exp. 3) at station JARE51-M on 5 January 2010. (b) ΔCO_2 indicates the change in CO_2 concentration inside the chamber since the chamber was closed. The regression lines were based on the data obtained after each measurement. The horizontal dashed line indicates $\Delta CO_2 = \pm 0$ ppm. The slope was expressed as ppm min^{-1}.

2.7. Sampling of Snow, Slush Water, Brine, Sea Ice, and Under-Ice Water

[17] Snow, collected for salinity measurements, was sampled every 10 cm using a polycarbonate shovel, and placed into polyethylene zip-lock bags. Snow samples were melted at room temperature (+20°C) in the laboratory. Snow temperatures and densities were measured in situ every 10 cm using a needle-type temperature sensor (Testo 110 NTC, Brandt Instruments, Inc., USA) and a snow density sampler (Climate Engineering, Niigata, Japan), respectively.

[18] In order to characterize the ice surface condition combined with snow depth and density, the water equivalent of snow was calculated by multiplying snow depth by snow density [*Jonas et al.*, 2009]. For stations where superimposed-ice was formed over the flooded slush layer, water equivalent of superimposed-ice was also evaluated. For the calculation of the water equivalent of superimposed-ice, a density of 862 kg m^{-3} was used based on sea ice measurements from the Ross Sea in summer [*Kawamura et al.*, 2004]. For the diurnal variation experiment from 18 to 19 January 2010, the temperature data logger (RTR 52, T & D Corp., Nagano, Japan) was installed in the top 2 cm of the snow (snow surface) and at the snow-sea ice interface (snow bottom). Snow sampling and measurements of snow temperature and density were examined at the downwind side and 2 m away from the CO_2 chambers.

[19] Flooded slush water was collected for salinity and dissolved inorganic carbon (DIC) measurements with a diaphragm pump (EWP-01, AS ONE Corporation, Osaka, Japan) via an attached Teflon tube connected to the installation hole of the chamber. For salinity measurements, samples were placed into 12 mL glass screw-cap vials (Nichiden-Rika Glass Co. Ltd, Kobe, Japan) during JARE51 and 100 mL polypropylene bottles (I-Boy, AS ONE Corporation, Osaka, Japan) during ICE11. For DIC measurements, samples were collected into 120 mL amber glass vials (Maruemu Co. Ltd, Osaka, Japan) during JARE51 and into 2 mL glass vials (Zinsser Analytics GmbH, Frankfurt, Germany) during ICE11. Immediately after DIC sampling, a 6.0% (wt.) mercury chloride ($HgCl_2$) solution (200 µL for a 120 mL vial and 5 µL for a 2 mL vial) was added to stop biological activity. Samples were stored in a refrigerator (+4°C) until analysis. Slush water temperature was measured in situ by the same sensor as described for snow above. For diurnal variations in CO_2 flux, the slush water temperature was measured continuously by the same data logger as described for snow above.

[20] Near-surface brine was collected at nonflooded sea ice surface at stations ICE11–21 and 22 using the sack hole method [*Gleitz et al.*, 1995]. The sack holes (25 and 50 cm deep) were drilled using an ice corer with an inner diameter of 9 cm (Mark II coring system, KOVACS Enterprises, Inc., Lebanon, NH, USA). The sack holes were covered with a 5 cm thick urethane lid to reduce heat and gas transfer across the brine-atmosphere interface. After the brine accumulated at the bottom of the hole over a period of approximately 10–15 min, the brine was pumped with a diaphragm pump and sampled for salinity and DIC in the same manner as for the slush water above. Brine temperature was measured in situ by the same sensor as described for snow above.

[21] Sea ice was collected at the same location as snow and was characterized for temperature, salinity, and ice texture. Immediately after collection of the first ice core, temperature was measured by inserting the same sensor as described for snow in holes drilled at 10 cm interval into the core, and the whole core transferred into a polyethylene bag and stored in a freezer (−20°C) for texture analysis. A second ice core for salinity measurement was also collected within 10 cm of the sea ice texture and temperature core and cut into 10 cm sections with a stainless steel saw and the ice sections placed into polyethylene zip-lock bags. Sea ice samples for salinity measurements were melted at room temperature (+20°C) in the laboratory and stored in the same manner as the slush water samples.

[22] Under-ice water samples were collected 1 m below the bottom of the sea ice for salinity and DIC measurements through an ice core hole with a Teflon water sampler (GL Science Inc., Tokyo, Japan). Samples were treated in the same manner as for the slush water above. Water temperature was measured immediately after water collection by inserting the same sensor as described for snow.

2.8. Sample Analysis, Calculation, and Thin Section Analysis

[23] The salinity of melted snow and sea ice, slush water, brine, and under-ice water was measured with a salinity analyzer (SAT-210, Toa Electronics Ltd., Tokyo, Japan) for the samples collected during JARE51 and a conductivity sensor (Cond 315i, WTW Wissenschaftlich-Technische

Werkstätten GmbH, Weilheim, Germany) during ICE11. Measurements were calibrated with International Association for the Physical Sciences of the Oceans (IAPSO) standard seawater (P series; Ocean Scientific International Ltd, Havant, UK).

[24] The DIC of slush water, brine, and under-ice water was determined by coulometry [*Johnson et al*. 1985] using a coulometer (CM5012, UIC Inc., Binghamton, NY, USA) for the samples collected during JARE51. Measurements were calibrated by using reference materials for seawater (Batch AG; KANSO Technos Co., Ltd., Osaka, Japan) traceable to the Certified Reference Material distributed by Prof. A. G. Dickson (Scripps Institution of Oceanography, La Jolla, CA, USA). For the samples collected during ICE11, DIC was determined with the flow injection method [*Hall and Aller*, 1992] using a conductivity detector (Model 1056, Amber Science Inc., Eugene, OR, USA). Measurements were calibrated by standards made from Sodium Hydrogen Carbonate (CAS-No. 144-55-8, AppliChem GmbH, Darmstadt, Germany).

[25] Brine volume of sea ice was calculated from the temperature and salinity of sea ice according to *Cox and Weeks* [1983] for temperature below −2°C, and according to *Leppäranta and Manninen* [1988] for temperatures within the range 0 to −2°C.

[26] For sea ice texture analysis, the ice core was split in half lengthwise with an electric band saw and sliced in sections of 0.7 cm thickness in a cold room (−20°C). Each ice section was attached to a glass plate and further sliced to a thickness of 0.1 cm with a microtome (Model SM2400, Leica Microsystems, Wetzlar, Germany). The ice crystallographic structures were photographed by illuminating the thin sections under polarized light. Based on the photographs, ice texture was categorized as granular, columnar, or a mixture of granular and columnar ice (g/c) [*Eicken and Lange*, 1989].

3. Results

3.1. Characteristics of Snow and Sea Ice

[27] The characteristics of snow and sea ice are summarized in Tables 1 and 2. The thickness of snow and sea ice ranged between 1.0 and 68.0 and 31.0 and 430.0 cm, respectively (Table 1). The sea ice surface was flooded both during JARE51 and ICE11 and a slush layer of 6.0−38.0 cm depth was observed. During JARE51 the thickness of the superimposed-ice layer ranged from 6.0 to 15.0 cm (Table 1). Snow and the upper 20 cm of the sea ice were relatively warm, particularly during JARE51, ranging from −1.1 to +0.6°C (Table 2). Snow salinity was zero during JARE51, while higher snow salinities of up to 18 were observed at the snow bottom during ICE11. Sea ice salinity was generally low for Antarctic fast ice, ranging from 0.0 to 2.0, compared to Arctic first-year pack ice, ranging from 4.1 to 10.6 (Table 2). Snow density and water equivalent (snow and superimposed-ice combined) was 297.0−545.2 and 57.2−420.3 kg m^{-2}, respectively, and values for Antarctic fast ice were generally higher than those for Arctic pack ice. Brine volume fraction varied from 2.1 to 31.6% with higher values observed for Arctic pack ice (Table 2).

[28] At all stations collected during JARE51-M (19 January 2010), and ICE11, vertical thin sections of ice cores showed that granular ice composed less than 21.0%, while columnar ice dominated the middle and lower parts of the cores (72.6−100.0%) for the samples collected (Figure 4).

3.2. Physicochemical Properties of Slush Water, Brine, and Under-Ice Water

[29] Temperature, salinity, and DIC of slush water, brine, and under-ice water are summarized in Table 3. Slush water temperatures, ranging from −1.8 to +3.2°C, were generally warmer than those measured in the under-ice water column (range from −1.8 to −0.3°C). Slush water salinity varied from 4.6 to 45.5, while salinity of under-ice water was relatively constant (33.5 ± 0.7) (mean ± 1SD). DIC ranged widely for slush water (199.1−3136.3 μmol kg^{-1}), while DIC was relatively constant for the under-ice water (2113.0 ± 103.1 μmol kg^{-1}). Generally, Antarctic slush waters were characterized by higher temperature and lower salinity and DIC than those for the Arctic (Table 3). For the brine samples (25 and 50 cm depth) collected at stations ICE11–21 and 22 for the Arctic ice, temperature (<−3.6°C) was much lower and salinity (>66.8) and DIC (>3812.1 μmol kg^{-1}) were much higher than those for the slush layer and under-ice water column.

3.3. CO_2 Flux

[30] The air-sea ice CO_2 fluxes of all measurements obtained for the different ice surfaces ranged from −4.0 to +0.5 mmol C m^{-2} d^{-1}. Table 4 summarizes the CO_2 flux measurements for each surface. The mean CO_2 flux measured over the snow surface (F_{snow}) was −0.2 ± 0.3 mmol C m^{-2} d^{-1}, and a similar mean flux value measured over the bare ice surface (F_{ice}) (−0.1 ± 0.2 mmol C m^{-2} d^{-1}). On average higher negative CO_2 fluxes were obtained for the flooded slush surface (F_{flood}) (−1.1 ± 0.9 mmol C m^{-2} d^{-1}), with peak values as high as −4.0 mmol C m^{-2} d^{-1}. The ratio F_{snow}/F_{flood} ranged from 0.1 to 0.5 (Table 4).

[31] The F_{snow}/F_{flood} ratio was strongly correlated with water equivalent of snow ($r^2 = 0.88$, $p < 0.006$), superimposed-ice ($r^2 = 0.99$, $p < 0.004$), and snow and superimposed-ice combined ($r^2 = 0.95$, $p < 0.002$) (Figure 5). The F_{snow}/F_{flood} ratios decreased with increasing water equivalent (Figure 5).

3.4. Temporal Variation in CO_2 Flux

[32] Temporal variation in snow, slush water, and under-ice water properties and CO_2 flux was examined between 2 and 19 January 2010 at the JARE51-M time series station (Figure 6). During the study period, thickness of snow and superimposed-ice decreased with time from 34.0 to 9.0 and 13.0 to 6.0 cm, respectively (Figure 6a and Table 1). On the other hand, snow temperature and snow density increased with time from +0.1 to +0.5°C and 445.3 to 506.1 kg m^{-3}, respectively (Figure 6b and Table 2). Variations in water equivalent of snow and superimposed-ice combined were similar to those in snow depth, which decreased from 261.0 to 97.3 kg m^{-2} during the study period (Figure 6c and Table 2).

[33] Salinity of slush water decreased significantly from 27.4 to 7.6 during the study period while salinity of under-ice water was almost constant at 33.2 ± 0.8 (Figure 6d and Table 3). Moreover, the temporal variations in DIC of slush water and under-ice water were similar to

Table 2. Snow Temperature, Salinity, Density, and Water Equivalent[a]

Station	Date	Snow				Sea Ice (top 20 cm)		
		Temperature (°C)	Salinity	Density (kg m^{-3})	Water Equivalent (kg m^{-2})[b]	Temperature (°C)	Salinity	Brine Volume Fraction (%)
JARE51-M	2 Jan 2010	+0.2 (+0.1 to +0.3)	0.0 (0.0 to 0.0)	445.3 (355.1 to 499.7)	245.7	−0.6 (−0.9 to −0.2)	1.3 (0.5 to 2.0)	10.6
JARE51-M	5 Jan 2010	+0.1 (−0.1 to +0.5)	0.0 (0.0 to 0.0)	488.7 (486.1 to 491.7)	261.0	−0.2 (−0.3 to −0.1)	0.2 (0.2 to 0.2)	5.0
JARE51-M	11 Jan 2010	+0.5 (+0.5 to +0.5)	0.0 (0.0 to 0.0)	505.1 (472.3 to 545.2)	229.1	−0.2 (−0.4 to ±0.0)	0.1 (0.1 to 0.2)	2.5
JARE51-M	19 Jan 2010	+0.5 (+0.4 to +0.6)	0.0 (0.0 to 0.0)	506.1 (462.0 to 528.1)	97.3	−0.7 (−0.7 to −0.6)	0.3 (0.0 to 0.6)	2.1
JARE51-S	10 Feb 2010	−0.1 (−0.2 to ±0.0)	0.0 (0.0 to 0.0)	427.9 (377.2 to 487.5)	420.3	−0.4 (−1.1 to ±0.0)	0.4[c]	4.9
ICE11-11	29 and 30 Apr 2011[d]	−2.2 (−2.7 to −1.8)	2.3 (0.0 to 5.5)	381.2 (363.0 to 399.3)	57.2	−3.3 (−3.5 to −3.1)	8.1 (7.9 to 8.3)	12.0
ICE11–20	2 May 2011	−0.5 (−1.5 to ±0.0)	1.3 (0.0 to 2.5)	394.4 (392.7 to 396.0)	77.3	−2.0 (−2.0 to −1.9)	9.5 (8.4 to 10.6)	23.8
ICE11–21	3 May 2011	−2.2 (−3.2 to −1.9)	6.0 (0.0 to 18.0)	326.7 (297.0 to 359.7)	81.7	−3.9 (−4.1 to −3.7)	7.7 (6.3 to 9.0)	9.7
ICE11–22	6 May 2011	−2.4 (−3.4 to −0.1)	2.4 (0.0 to 7.1)	396.0 (303.6 to 488.4)	118.8	−3.8 (−3.9 to −3.5)	8.3 (7.8 to 8.8)	10.8
ICE11–27b	11 May 2011	−3.3[c]	_[e]	_[e]	_[e]	−0.9 (−0.9 to −0.8)	5.7 (4.1 to 7.0)	31.6

[a]Sea ice temperature, salinity, and brine volume fraction for the top 20 cm. The range is indicated in brackets.
[b]Water equivalent of superimposed-ice was included if superimposed-ice was formed over the slush layer.
[c]Only one data.
[d]Sea ice coring and snow observations were performed on 29 and 30 January 2011, respectively.
[e]"_" indicates no data.

those in salinity of slush water and under-ice (Figures 6d and 6e). DIC in the slush water decreased significantly from 1529.6 to 318.1 μmol kg^{-1}, while DIC in the under-ice water was almost constant at 2031.3 ± 80.4 (Figure 6e and Table 3). Temporal variations of salinity and DIC in slush water were highly correlated ($r^2 = 0.99$, $p < 0.002$) (Figure 7). F_{flood} changed from −2.3 to −0.5 mmol C m^{-2} d^{-1}, while F_{snow} was almost constant (−0.2 ± 0.3 mmol C m^{-2} d^{-1}) during the study period (Figure 6f and Table 4).

3.5. Diurnal Observations

[34] The continuous diurnal measurements of air, snow, and slush water temperature, solar radiation, salinity, and

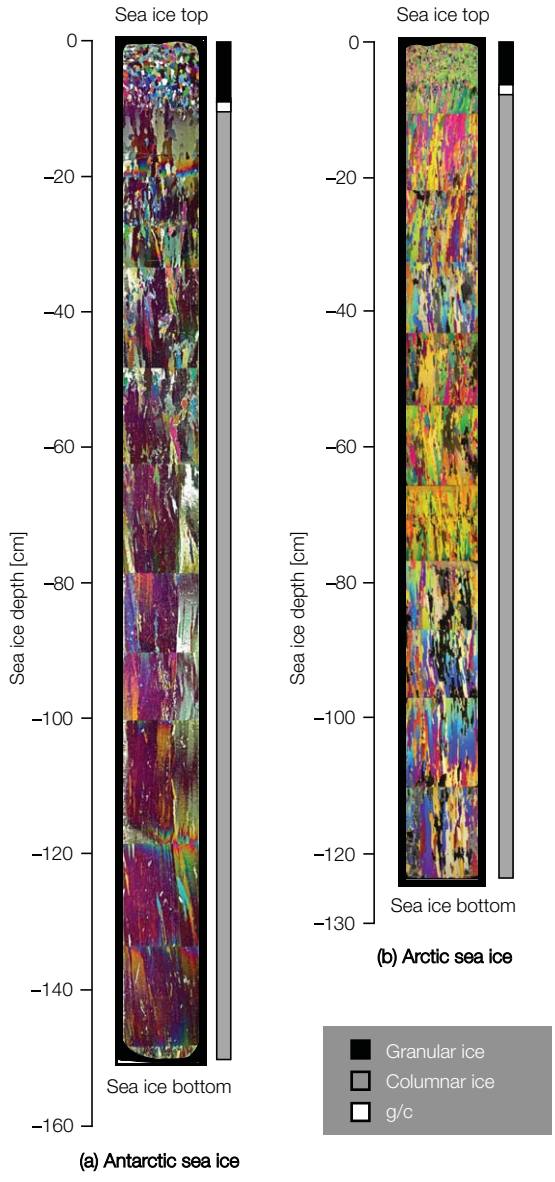

Figure 4. Photographs of ice core thin sections in polarized light for (a) the Antarctic sea ice at station JARE51-M on 19 January 2010 and (b) the Arctic sea ice at station ICE11–21 on 3 May 2011. The g/c indicates the mixture of granular and columnar ice.

Table 3. Temperature, Salinity, and DIC for Slush Water, Brine, and Under-Ice Water[a]

		Slush Water			Brine			Under-Ice Water[b]		
Station	Date	Temperature (°C)	Salinity	DIC (μmol kg^{-1})	Temperature (°C)	Salinity	DIC (μmol kg^{-1})	Temperature (°C)	Salinity	DIC (μmol kg^{-1})
JARE51-M	2 Jan 2010	−0.6 (−0.6 to −0.6)	27.4 (25.4 to 29.3)	1529.6 (1448.9 to 1610.2)	_[c]	_[c]	_[c]	−1.8	34.1	2116.9
JARE51-M	5 Jan 2010	−0.6 (−1.0 to −0.1)	19.0 (16.1 to 21.9)	1010.3 (842.1 to 1178.5)	_[c]	_[c]	_[c]	−1.3	33.6	2079.4
JARE51-M	11 Jan 2010	+2.2 (+1.9 to +2.4)	11.0 (10.7 to 11.2)	610.0 (593.9 to 626.1)	_[c]	_[c]	_[c]	−0.3	32.7	1944.1
JARE51-M	18 and 19 Jan 2010[d]	+1.1 (−0.8 to +3.2)	7.6 (4.6 to 10.1)	318.1 (199.1 to 548.6)	_[c]	_[c]	_[c]	_[c]	32.3	1985.0
JARE51-S	10 Feb 2010	+0.7[b]	20.3[b]	1084.2[b]	_[c]	_[c]	_[c]	_[c]	34.2	2183.6
ICE11-11	30 Apr 2011	−1.7 (−1.8 to −1.7)	45.1 (44.7 to 45.5)	3100.2 (3064.0 to 3136.3)	_[c]	_[c]	_[c]	−1.6	33.8	2214.1
ICE11–20	2 May 2011	−1.4 (−1.5 to −1.3)	40.2 (39.9 to 40.4)	2604.5 (2581.4 to 2627.6)	_[c]	_[c]	_[c]	−1.0	33.5	2167.2
ICE11–21	3 May 2011	_[c]	_[c]	_[c]	−3.9 (−3.9 to −3.8)	78.3 (77.6 to 79.6)	3999.0 (3863.4 to 4132.5)	_[c]	_[c]	_[c]
ICE11–22	6 May 2011	_[c]	_[c]	_[c]	−3.8 (−4.0 to −3.6)	68.7 (66.8 to 71.4)	3873.7 (3812.1 to 3917.6)	−1.4	33.9	2213.9
ICE11–27b	11 May 2011	−1.7 (−1.7 to −1.6)	38.9 (38.5 to 39.3)	2559.7 (2513.3 to 2606.2)	_[c]	_[c]	_[c]	_[c]	_[c]	_[c]

[a]The range is indicated in brackets.
[b]Only one data.
[c]"_" means no data.
[d]Slush observations were obtained from 18 to 19 January 2010 (every 6 h). Under-ice water was sampled on 19 January 2010.

DIC in slush water and CO_2 flux were obtained between 18 and 19 January 2010 at the JARE51-M time series station (Figure 8). Air temperature fluctuated from +0.1 to +2.9°C over the daily cycle, in synchrony with the fluctuations in solar radiation ranging from 5.6 to 783.3 W m^{-2} (Figure 8a). Temperature of snow and slush water also changed in synchrony (Figure 8b) with the fluctuations in solar radiation and air temperature (Figure 8a). Snow temperature at the surface changed dramatically compared to those at the snow bottom and slush water, and reached up to +1.3°C at the snow surface (Figure 8b).

[35] Salinity and DIC in slush water decreased with time from 10.1 to 4.6 and 548.6 to 224.4 μmol kg^{-1}, respectively, during the study period (Figure 8c), and they were highly correlated ($r^2 = 0.84$, $p < 0.03$) (Figure 7). F_{snow} and F_{flood} changed in synchrony with the fluctuations in solar radiation and temperature of air, snow, and slush layer, ranging from −0.7 to +0.2 mmol C m^{-2} d^{-1} for F_{snow} and from −1.5 to −0.2 mmol C m^{-2} d^{-1} for F_{flood} (Figure 8d).

4. Discussion

[36] During both studies in the Antarctic and Arctic, snow and sea ice were relatively warm and the sea ice surface frequently flooded due to heavy snow cover (Tables 1 and 2). In addition, meltwater supply to the ice surface from melting snow and ice surface also contributed to the formation of a flooded surface layer (Figures 6 and 8 and Table 3). Formation of a flooded slush surface has been widely observed in heavily snow covered sea ice during the ice melting season [*Haas et al*., 2001; *Kattner et al*., 2004; *Ackley et al*., 2008; *Zemmelink et al*., 2006, 2008; *Papadimitriou et al*., 2009; *Nomura et al*., 2012, 2013]. High biological activity [*Kattner et al*., 2004] and meltwater supply from the melting snow and sea ice [*Nomura et al*., 2012] alter salinity and DIC in the flooded slush surface (Figures 6–8 and Table 3).

[37] The strong correlation between slush water salinity and DIC observed during the JARE51 time series study (Figure 7) indicated that the dilution effect by the freshwater supply from melting snow and sea ice, was primarily responsible for the variations of the chemical components in the slush water. A similar relationship was observed in the same season and area over the land-fast multiyear sea ice station in Lützow-Holm Bay, Antarctica [*Nomura et al*., 2012], showing that DMS concentrations in the slush water decreased dramatically with decreasing salinity. In comparison, salinity and DIC in under-ice water were almost constant during the study period (Figure 6 and Table 3). These results suggest that melting of snow and the ice surface did not affect the under-ice water properties. Water exchange between sea ice and the under-ice water column can be mediated through well-developed brine channels in sea ice [*Tison et al*., 2008; *Nomura et al*., 2009]. However, the different patterns in salinity and DIC for slush and under-ice water (Figure 6 and Table 3) suggests that there was no linkage between slush and under-ice water, and that the slush water, dominating at the top of sea ice, was isolated from the brine under-ice water system during the time of observations.

[38] The air-sea ice CO_2 flux examined over various surface types clearly show that the physical conditions at the

Table 4. CO_2 Flux Measured Over the Snow (F_{snow}), Ice Surface (F_{ice}), and Flooded Slush Surface (F_{flood}), and the F_{snow}/F_{flood} Ratio

Station	Date	CO_2 Flux (mmol C m^{-2} d^{-1}) (mean ± 1 SD)			F_{snow}/F_{flood}[a]
		F_{snow}	F_{ice}	F_{flood}	
JARE51-M	2 Jan 2010	+0.1 ± 0.1	–[b]	−2.3 ± 0.8	–[b]
JARE51-M	5 Jan 2010	−0.2 ± 0.2	−0.1 ± 0.3	−2.2 ± 0.6	0.1
JARE51-M	11 Jan 2010	−0.3 ± 0.2	–[b]	−1.8 ± 0.6	0.2
JARE51-M	18 and 19 Jan 2010	−0.2 ± 0.3	–[b]	−0.5 ± 0.5	0.4
JARE51-S	10 Feb 2010	−0.1 ± 0.0	−0.1 ± 0.1	−2.2 ± 0.5	0.1
ICE11-11	30 Apr 2011	−0.6[c]	–[b]	−1.2 ± 0.3	0.5
ICE11–20	2 May 2011	−0.4 ± 0.4	–[b]	−0.8 ± 0.4	0.5
ICE11–21	3 May 2011	+0.1 ± 0.2	±0.0 ± 0.2	–[b]	–[b]
ICE11–22	6 May 2011	±0.0 ± 0.2	−0.1 ± 0.2	–[b]	–[b]
ICE11–27b	11 May 2011	−0.4 ± 0.1	–[b]	−1.0 ± 0.7	0.4
Mean for all measurements		−0.2 ± 0.3	−0.1 ± 0.2	−1.1 ± 0.9	0.3

[a]When F_{snow} was positive, F_{snow}/F_{flood} was not estimated.
[b]"–" means no data.
[c]Only one data.

sea ice surface affect the magnitude of air-sea ice CO_2 flux (Figures 5, 6, and 8 and Table 4). The CO_2 flux measured directly over the flooded slush surface (F_{flood}) constituted a net CO_2 sink with −1.1 ± 0.9 mmol C m^{-2} d^{-1}, which was an order of magnitude higher than the flux measured over the snow surface (F_{snow}: −0.2 ± 0.3 mmol C m^{-2} d^{-1}) and nonflooded bare sea ice surface (F_{ice}: −0.1 ± 0.2 mmol C m^{-2} d^{-1}) (Table 4), illustrating that the flooded slush surface acts as sink for atmospheric CO_2. A sea ice CO_2 sink was previously reported by *Zemmelink et al.* [2006], who showed that CO_2 was absorbed by multiyear ice in the Weddell Sea, and that the higher negative CO_2 flux (−18.2 to −4.6 mmol C m^{-2} d^{-1}), measured by the eddy covariance method, was driven by biological uptake within the flooded slush layer at the snow-sea ice interface. In comparison, during JARE51 and ICE11, Chlorophyll-*a* concentrations were low (<1.1 μg L^{-1}) at the top of sea ice [*Nomura et al.*, 2013] and slush layer [*Nomura et al.*, 2012] observed in the same season and area as this study.

[39] F_{snow} and F_{ice} were less negative than F_{flood} (Table 4). Furthermore, the F_{snow}/F_{flood} ratio ranged from 0.1 to 0.5 (Table 4), illustrating that 50–90% of the potential CO_2 flux across the flooded slush surface was reduced due to the presence of the snow and/or superimposed-ice. Previous studies have shown that snow accumulation and formation of superimposed-ice over sea ice effectively impede CO_2 [*Delille*, 2006; *Nomura et al.*, 2010a] and DMS [*Nomura et al.*, 2012] gas exchange. *Nomura et al.* [2010a] reported that snow thicknesses higher than about 9 cm effectively shut down CO_2 exchange between air and sea ice. Other studies examined the CO_2 exchange through snow pack deposited over soils [*Sommerfeld et al.*, 1993, 1996; *Winston et al.*, 1995; *Takagi et al.*, 2005; *Elberling*, 2007; *Schindlbacher et al.*, 2007; *Bowling and Massman*, 2011] and gas dynamics within the firn layer on the top of glacier [*Ikeda-Fukazawa et al.*, 2005; *Kawamura et al.*, 2006]. These studies concluded that the snow cover is a porous medium for gas. However, in some cases, the snow properties (e.g., thickness, density, and presence of an ice layer in the snow) are also important factors contributing to the gas exchange processes in snow [e.g., *Schindlbacher et al.*, 2007]. Therefore, in our study, a new parameter "water equivalent" that combines thickness with density of snow and superimposed-ice was used as an indicator for the snow and superimposed-ice properties and ice surface conditions (Table 2). A strong relationship between the F_{snow}/F_{flood} ratio and water equivalent (Figure 5) suggests that the CO_2 flux is clearly affected by snow and superimposed-ice properties.

[40] Without removing the snow over the flooded slush surface, more negative F_{snow} (−0.6 to −0.4 mmol C m^{-2} d^{-1}) was measured for Arctic sea ice (Table 4), where the snow bottom was flooded (Table 1). Because snow thickness and density were generally low for Arctic stations

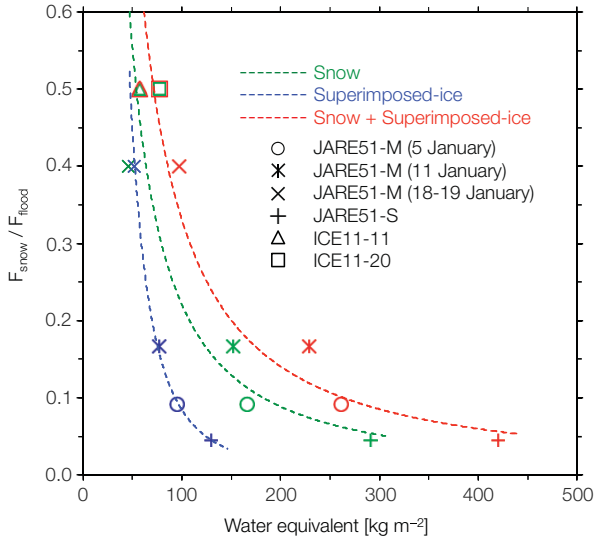

Figure 5. Relationships between the F_{snow}/F_{flood} ratio and water equivalent of snow (green symbol and dashed line), superimposed-ice (blue symbol and dashed line), and snow and superimposed-ice combined (red symbol and dashed line). Symbols represent JARE51-M (circle: 5 January 2010, star: 11 January 2010, cross: 18 and 19 January 2010), JARE51-S (plus), ICE11-11 (triangle), and ICE11–20 (square). Dashed lines indicate the fitting curve used to describe the relationship.

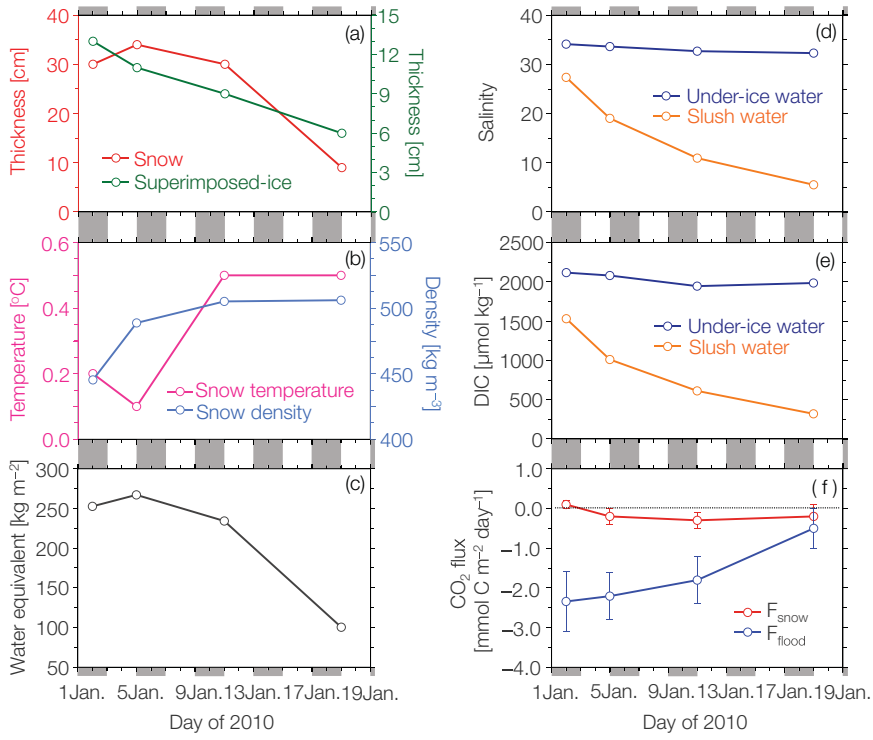

Figure 6. Temporal variations of (a) snow and superimposed-ice thickness, (b) temperature and density of snow, (c) water equivalent, (d) salinity of slush and under-ice water, (e) DIC in slush and under-ice water, and (f) CO_2 flux, during JARE51. The horizontal dashed line in Figure 6f indicates CO_2 flux $= \pm 0$ mmol C m^{-2} d^{-1}.

(Tables 1 and 2), the water equivalent was also low compared to Antarctic stations (Table 2). The F_{snow}/F_{flood} ratio for Arctic sea ice was thus higher than for Antarctic sea ice (Figure 5 and Table 4). Thus, the gas exchange occurred more effectively from the flooded surface through the snow in the Arctic. In addition, no superimposed-ice was found between the snow and slush layer in Arctic (Table 1). Because superimposed-ice had a low salinity [*Nomura et al.*, 2012] and high density [*Kawamura et al.*, 2004], one

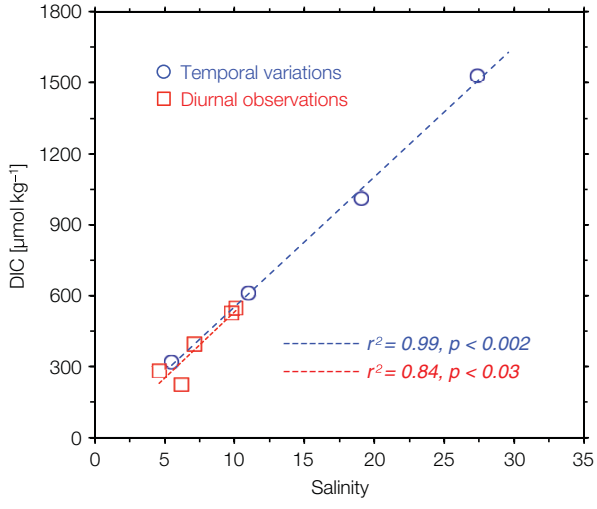

Figure 7. Relationship between the DIC and salinity for temporal variations (blue symbol and dashed line) and diurnal observations (red symbol and dashed line) during JARE51. Dashed lines indicate the fitting curve used to describe the relationship.

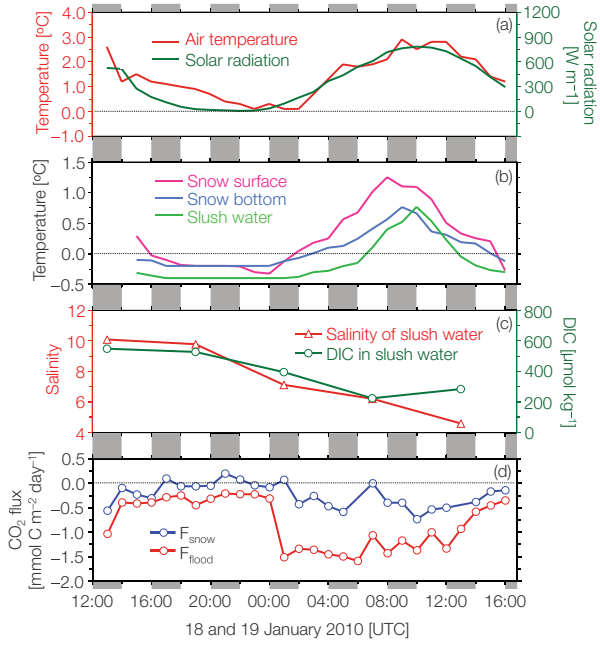

Figure 8. Diurnal variations of (a) air temperature and solar radiation, (b) snow temperature, (c) salinity and DIC in slush water, and (d) CO_2 flux, during JARE51. The horizontal dashed lines indicate zero for each parameter.

can expect that the presence of a superimposed-ice layer prevents CO_2 exchange between flooded slush and the atmosphere in Antarctic sea ice as observed in the present study (Table 4) and previous studies [*Delille*, 2006; *Nomura et al*., 2010a, 2012].

[41] Our temporal and diurnal experiments (Figures 6 and 8) clearly indicated that the CO_2 flux varied according to variations in the sea ice surface properties. During the temporal study, thickness of snow and superimposed-ice decreased while snow density increased with warming and melting (Figures 6a and 6b), and water equivalent decreased with time (Figure 6c). These changes in sea ice surface properties were clearly reflected in the increase of the F_{snow}/F_{flood} ratio from 0.1 on 5 January to 0.4 on 19 January 2010 (Table 4), and in the slight decrease of F_{snow} from +0.1 to −0.2 mmol C m^{-2} d^{-1} (Figure 6f and Table 4). Similar results were also observed for the diurnal variation experiment (Figure 8). Air and snow temperatures changed in synchrony with fluctuations in solar radiation (Figures 8a and 8b). During daytime around 08:00 (universal time coordinated (UTC)) on 19 February 2010, snow temperatures of up to ±0°C (Figure 8b), resulted in snow melting and downward transport of meltwater through channels in the snow [*Sommerfeld et al*., 1991; *Katsushima et al*., 2009]. In addition, *Sommerfeld et al*. [1991] reported that the onset of snow melting and meltwater transport affect the CO_2 dynamics within the snowpack. Diurnal variations showed that F_{snow} changed from almost zero flux on 18 February to fluxes of up to −0.7 mmol C m^{-2} d^{-1} between 00:00 and 16:00 (UTC) on 19 February 2010 in synchrony with fluctuations in solar radiation and air and snow temperatures (Figure 8). These results suggest that snowmelt would affect the CO_2 dynamics within snow and the air-sea ice CO_2 flux, possibly through the well-developed channel system formed during downward transport of meltwater within snow.

[42] Variations in CO_2 flux, especially in F_{flood}, will depend on variations in biogeochemical properties of slush water because F_{flood} was measured directly over the flooded slush surface. pCO_2 at the surface of sea ice is an important factor controlling the air-sea ice CO_2 flux [*Delille*, 2006; *Nomura et al*., 2006, 2010a]. Although we did not obtain pCO_2 data for the slush water layer in this study, the variations of DIC and salinity at the top of sea ice (slush water and brine) (Figure 7) can help to understand pCO_2 dynamics [*Nomura et al*., 2010a]. The pCO_2 in the top of sea ice (in brine) changes dramatically from sea ice formation to the melting season [*Delille*, 2006; *Nomura et al*., 2006, 2010a, *Miller et al*., 2011b; *Geilfus et al*., 2012; *Papadimitriou et al*., 2012]. During sea ice formation, pCO_2 increases with increases in DIC, and with changes in CO_2 solubility and the dissociation constants of carbonic acid as a function of salinity [*Weiss*, 1974; *DOE*, 1994; *Millero*, 1995], which increases as a result of the progressive rejection of dissolved impurities from growing ice [*Nomura et al*., 2006]. Therefore, generally, pCO_2 in sea ice (brine) is supersaturated with respect to the air during periods of ice growth. On the other hand, during ice melt, the same process occurs for pCO_2 due to the dilution effect, but in the opposite direction (decrease in pCO_2 with decreases in DIC). In the case of flooded slush surfaces, these relationships could be the same. The snow and sea ice were relatively warm during both JARE51 and ICE11, indicating that the ice was in the melting period, suggesting that pCO_2 in the slush water layer was low compared to the atmospheric partial pressure, and thus had the potential to absorb CO_2 from the atmosphere. In addition, our negative CO_2 flux and temporal variations of F_{flood} (Figures 6 and 8 and Table 4) clearly illustrated that the slush water layer was undersaturated in pCO_2 with respect to the atmosphere and variation of pCO_2 and salinity in slush water followed the variations in melting without any input of seawater. However, the pCO_2 in sea ice varies depending on other processes as well (e.g., carbonate chemistry, biological activity, and ikaite formation/dissolution). Therefore, further investigation will be required to understand the pCO_2 dynamics within the surface slush layer and its relation with the CO_2 flux.

[43] Our CO_2 fluxes ranged from −4.0 to +0.5 mmol C m^{-2} d^{-1} and fall within the range (−5.2 to +1.9 mmol C m^{-2} d^{-1}) reported from previous studies based on the chamber method [*Delille*, 2006; *Nomura et al*., 2010a, 2010b; *Geilfus et al*., 2012]. However, substantially higher CO_2 fluxes were measured by the eddy covariance method, ranging from −259.2 to +74.3 mmol C m^{-2} d^{-1} [*Zemmelink et al*., 2006; *Miller et al*., 2011a; *Papakyriakou and Miller*, 2011]. Direct comparison is further complicated because CO_2 flux measurements with both methods were performed at different seasons and surface conditions. One reason for the large difference between the chamber and eddy covariance methods is considered to be the differences in the footprint size of CO_2 exchange measured with the two approaches. The eddy covariance method reflects the average flux over a large area [*Zemmelink et al*., 2006, 2008; *Burba et al*., 2008; *Amiro*, 2010; *Miller et al*., 2011a; *Papakyriakou and Miller*, 2011], and it is, therefore, most useful for understanding large scale fluxes. However, it is difficult to distinguish the contribution from different surface types and local events [*Zemmelink et al*., 2006, 2008]. In addition, CO_2 flux measurements in cold weather condition by the open-path eddy covariance systems should be interpreted with caution, given that the fluxes may be prone to biases [*Burba et al*., 2008]. While the chamber method is useful for understanding the relationship between fluxes and ice surface conditions on small scales. Therefore, the different spatial scales of the two methods may be one reason for the discrepancy in CO_2 flux measurements. These methodological gaps are still being discussed and not yet fully understood by the CO_2 flux community [*Burba et al*., 2008; *Amiro*, 2010]. Furthermore, the CO_2 flux is influenced by wind-driven pressure pumping [*Takagi et al*., 2005; *Suzuki et al*., 2006; *Bowling and Massman*, 2011]. As a result, the magnitude of CO_2 fluxes through snow overlying soil [e.g., *Takagi et al*., 2005] or sea ice [e.g., *Papakyriakou and Miller*, 2011] increases with wind velocity and pressure pumping can enhance the transport beyond molecular diffusion by up to 40% [*Bowling and Massman*, 2011]. This suggests that the chamber method, driven by molecular diffusion, underestimates the CO_2 flux. We, however, collected samples only on days when wind speeds were low (e.g., Table 1) and wind-driven pressure pumping was small, thus minimizing wind effects on the measured CO_2 flux. Further evaluation of the impact of pressure pumping on CO_2 flux is urgently needed for sea ice.

[44] Our results suggest that Antarctic and Arctic sea ice is a potential sink for atmospheric CO_2 during the melt season, particularly the flooded ice surface due to the direct contact of the slush water layer with the atmosphere. It is important to note that the formation of a slush layer likely occurs frequently during spring melt [*Haas et al*., 2001; *Kattner et al*., 2004; *Ackley et al*., 2008; *Zemmelink et al*., 2006, 2008; *Papadimitriou et al*., 2009; *Nomura et al*., 2012, 2013]. The amount of CO_2 absorbed by flooded sea ice may therefore be a significant fraction of the total CO_2 uptake of the global ocean. Although few data are available thus far to support our conclusions we provide first evidence on how changes in sea ice properties amplified by ongoing climate change could impact air-sea ice CO_2 fluxes, particularly in the Arctic Ocean [*Parkinson and Cavalieri*, 2012]. During these processes, snowmelt on the sea ice and the subsequent formation of a flooded surface and surface melt ponds will be promoted due to changes in the ice surface energy budget [*Nicolaus et al*., 2012]. The effect of snow on the air-sea ice CO_2 flux decreased with decreasing snow amount over the sea ice (Figure 5), illustrating that if snow thickness decreases [*Screen and Simmonds*, 2011], air-sea ice CO_2 flux will be enhanced. In addition, formation of surface melt ponds [*Semiletov et al*., 2004] and carbon uptake by algae within melt ponds [*Lee et al*., 2012] could also contribute to CO_2 uptake. In the future, the melting of sea ice in polar oceans will strongly affect gas exchange processes although processes related to the freezing and melting of sea ice still represent large unknowns [*Parmentier et al*., 2013].

5. Conclusion

[45] In this study, we present evidence that melting and flooded Antarctic and Arctic sea ice acts as a sink for atmospheric CO_2. We used a newly developed CO_2 measuring system composed of three automatic open-close chambers, which allowed us to simultaneously evaluate the effect of different sea ice surfaces and conditions on air-sea ice CO_2 flux over different temporal scales.

[46] The CO_2 fluxes of all measurements ranged from -4.0 to $+0.5$ mmol C m^{-2} d^{-1}. After removing the snow/superimposed-ice, the CO_2 flux measured directly over the flooded sea ice surface (F_{flood}) constituted a net CO_2 sink with -1.1 ± 0.9 mmol C m^{-2} d^{-1} (mean $\pm$ 1SD), which was an order of magnitude higher than the flux measured over the snow surface (F_{snow}: -0.2 ± 0.3 mmol C m^{-2} d^{-1}) and nonflooded (bare) sea ice surface (F_{ice}: -0.1 ± 0.2 mmol C m^{-2} d^{-1}). The ratio F_{snow}/F_{flood} decreased with increasing water equivalent estimated from the density and thickness of snow/superimposed-ice, suggesting that the CO_2 flux through the ice surface is clearly affected by the properties of snow/superimposed-ice. The F_{snow}/F_{flood} ratio ranged from 0.1 to 0.5 for all sites, illustrating that 50–90% of the potential flux at the flooded surface was reduced due to the presence of snow/superimposed-ice. Our temporal and diurnal experiments indicated that the warming of the ice surface, due to the increase in solar radiation and temperature, led to a melting of snow/superimposed-ice over the flooded surface. Hence, F_{snow} changed from almost zero to -0.7 mmol C m^{-2} d^{-1}, following the transition of the ice surface properties according to changes in radiative forcing.

[47] Our CO_2 flux measurements obtained from sea ice in both hemispheres provides a useful baseline for future studies addressing the impact of increased ice melting and flooding in enhancing the air-sea ice CO_2 flux across rapidly changing polar oceans.

[48] **Acknowledgments.** We thank S. Nakatsubo, Y. Kodama, H. Fukushi, K.Fujita, and M. Fukuchi for their support in developing the automatic open-close chamber system. We also express our gratitude to H. Shinagawa, S. Chavanich, S. Koga, N. Koc, the crew of RV Lance, and members of the ICE11 cruise and the JARE51 expedition for their support in the field. Special thanks goes to Y. W. Watanabe, A. Boetius, and E. Weiz for providing support for DIC sample analyses. We also thank three anonymous reviewers for their useful comments. This study was supported by the Japan Society for the Promotion of Science (21810036, 23-207, 24-4175), the National Institute of Polar Research (GS2-2), the Fram Centre, and the Centre for Ice, Climate and Ecosystems (ICE) at the Norwegian Polar Institute.

References

Ackley, S. F., M. J. Lewis, C. H. Fritsen, and H. Xie (2008), Internal melting in Antarctic sea ice: Development of "gap layers", *Geophys. Res. Lett.*, *35*, L11503, doi:10.1029/2008GL033644.

Amiro, B. (2010), Estimating annual carbon dioxide eddy fluxes using open-path analysers for cold forest sites, *Agric. Forest Meteorol.*, *150*(15), 1366–1372.

Bates, N. R. (2006), Air–sea CO_2 fluxes and the continental shelf pump of carbon in the Chukchi Sea adjacent to the Arctic Ocean, *J. Geophys. Res.*, *111*, C10013, doi:10.1029/2005JC003083.

Bowling, D. R., and W. J. Massman (2011), Persistent wind-induced enhancement of diffusive CO_2 transport in a mountain forest snowpack, *J. Geophys. Res.*, *116*, G04006, doi:10.1029/2011JG001722.

Burba, G., D. McDermitt, A. Grelle, D. Anderson, L. Xu (2008), Addressing the influence of instrument surface heat exchange on the measurements of CO_2 flux from open-path gas analyzers, *Global Change Biol.*, *14*(8), 1854–1876.

Comiso, J. C. (2010), Variability and trends of the global sea ice cover, in *Sea Ice*, edited by D. N. Thomas and G. S. Dieckmann, 2nd ed., pp. 205–246, Wiley-Blackwell, Oxford.

Cox, G. F. N., and W. F. Weeks (1983), Equations for determining the gas and brine volumes in sea-ice samples, *J. Glaciol.*, *29*, 306–316.

Delille, B. (2006), Inorganic carbon dynamics and air-ice-sea CO_2 fluxes in the open and coastal waters of the Southern Ocean, PhD thesis, pp. 1–297, Univ. of Liége, Liége, Belgium.

Delille, B., B. Jourdain, A. V. Borges, J.-L. Tison, and D. Delille (2007), Biogas (CO_2, O_2, dimethylsulfide) dynamics in spring Antarctic fast ice, *Limnol. Oceanogr.*, *52*, 1367–1379.

Dieckmann, G. S., G. Nehrke, S. Papadimitriou, J. Göttlicher, R. Steininger, H. Kennedy, D. Wolf-Gladrow, and D. N. Thomas (2008), Calcium carbonate as ikaite crystals in Antarctic sea ice, *Geophys. Res. Lett.*, *35*, L08501, doi:10.1029/2008GL033540.

DOE (1994), *Handbook of Methods for the Analysis of the Various Parameters of the Carbon Dioxide System in Seawater*, Version 2, edited by A. G. Dickson and C. Goyet, ORNL/CDIAC-74, pp. 1–22, Oak Ridge Natl. Lab., Oak Ridge, Tenn.

Eicken, H., and M. A. Lange (1989), Development and properties of sea ice in the coastal regime of the southeastern Weddell Sea, *J. Geophys. Res.*, *94*, 8193–8206.

Elberling, B. (2007), Annual soil CO_2 effluxes in the high arctic: The role of snow thickness and vegetation type, *Soil Biol. Biochem.*, *39*, 646–654.

Else, B. G. T., T. N. Papakyriakou, M. G. Asplin, D. G. Barber, R. J. Galley, L. A. Miller, and A. Mucci (2013), Annual cycle of air–sea CO_2 exchange in an arctic polynya region, *Global Biogeochem. Cycles*, *27*, 388–398, doi:10.1002/gbc.20016.

Fransson, A., M. Chierici, P. L. Yager, and W. O. Smith Jr. (2011), Antarctic sea ice carbon dioxide system and controls, *J. Geophys. Res.*, *116*, C12035, doi:10.1029/2010JC006844.

Geilfus, N.-X., G. Carnat, T. Papakyriakou, J.-L. Tison, B. Else, H. Thomas, E. Shadwick, and B. Delille (2012), Dynamics of pCO_2 and related air–ice CO_2 fluxes in the Arctic coastal zone (Amundsen Gulf,

Beaufort Sea), *J. Geophys. Res.*, *117*, C00G10, doi:10.1029/2011JC007118.

Gleitz, M., M. R. Vonderlo, D. N. Tomas, G. S. Dieckmann, and F. J. Millero (1995), Comparison of summer and winter inorganic carbon, oxygen and nutrient concentrations in Antarctic sea ice brine, *Mar. Chem.*, *51*, 81–89.

Golden, K. M., S. F. Ackley, and V. I. Lytle (1998), The percolation phase transition in sea ice, *Science*, *282*, 2238–2241.

Haas, C., D. N. Thomas, and J. Bareiss (2001), Surface properties and processes of perennial Antarctic sea ice in summer, *J. Glaciol.*, *47*,(159), 613–625.

Hall, O. J., and R. C. Aller (1992), Rapid, small volume, flow injection analysis for CO_2 and NH_4^+ in marine and fresh waters, *Limnol. Oceanogr.*, *37*(5), 1113–1119.

Ikeda-Fukazawa, T., K. Fukumizu, K. Kawamura, S. Aoki, T. Nakazawa, and T. Hondoh (2005), Effects of molecular diffusion on trapped gas composition in polar ice cores, *Earth Planet. Sci. Lett.*, *229*(3–4), 183–192.

Inoue, H. Y., and M. Ishii (2005), Variations and trends of CO_2 in the surface seawater in the Southern Ocean south of Australia between 1969 and 2002, *Tellus, Ser. B*, *57*, 58–69.

Johnson, K. M., A. E. King, and J. M. Sieburth (1985), Coulometric TCO_2 analyses for marine studies: An introduction, *Mar. Chem.*, *16*, 61–82.

Jonas, T., C. Marty, and J. Magnusson (2009), Estimating the snow water equivalent from snow depth measurements in the Swiss Alps, *J. Hydrol.*, *378*, 161–167.

Katsushima, T., T. Kumakura, and Y. Takeuchi (2009), A multiple snow layer model including a parameterization of vertical water channel process in snowpack, *Cold Reg. Sci. Technol.*, *59*, 143–151.

Kattner, G., D. N. Thomas, C. Haas, H. Kennedy, and G. S. Dieckmann (2004), Surface ice and gap layers in Antarctic sea ice: Highly productive habitats, *Mar. Ecol. Prog. Ser.*, *277*, 1–12.

Kawamura, K., J. P. Severinghaus, S. Ishidoya, S. Sugawara, G. Hashida, H. Motoyama, Y. Fujii, S. Aoki, and T. Nakazawa (2006), Convective mixing of air in firn at four polar sites, *Earth Planet. Sci. Lett.*, *244*, 672–682.

Kawamura, T., M. Jeffries, J.-L. Tison, and H. R. Krouse (2004), Superimposed-ice formation in summer on Ross Sea pack-ice floes, *Ann. Glaciol.*, *39*, 563–568.

Lee, S. H., D. A. Stockwell, H.-M. Joo, Y. Son, C.-K. Kang, and T. E. E. Whitledge (2012), Phytoplankton production from melting ponds on Arctic sea ice, *J. Geophys. Res.*, *117*, C04030, doi:10.1029/2011JC007717.

Leppäranta, M., and T. Manninen (1988), The brine and gas content of sea ice with attention to low salinities and high temperatures, *Internal Rep. 1988-2*, 15 pp., Finnish Inst. of Mar. Res., Helsinki, Finland.

Loose, B., W. R. McGillis, P. Schlosser, D. Perovich, and T. Takahashi (2009), Effects of freezing, growth, and ice cover on gas transport processes in laboratory seawater experiments, *Geophys. Res. Lett.*, *36*, L05603, doi:10.1029/2008GL036318.

McNeil, B. I., N. Metzl, R. M. Key, R. J. Matear, and A. Corbiere (2007), An empirical estimate of the Southern Ocean air-sea CO_2 flux, *Global Biogeochem. Cycles*, *21*, GB3011, doi:10.1029/2007GB002991.

Miller, L. A., T. N. Papakyriakou, R. E. Collins, J. W. Deming, J. K. Ehn, R. W. Macdonald, A. Mucci, O. Owens, M. Raudsepp, and N. Sutherland (2011a), Carbon dynamics in sea ice: A winter flux time series, *J. Geophys. Res.*, *116*, C02028, doi:10.1029/2009JC006058.

Miller, L. A., G. Carnat, B. G. T. Else, N. Sutherland, and T. N. Papakyriakou (2011b), Carbonate system evolution at the Arctic Ocean surface during autumn freeze-up, *J. Geophys. Res.*, *116*, C C00G04, doi:10.1029/2011JC007143.

Millero, F. J. (1995), Thermodynamic of the carbon dioxide system in the oceans, *Geochim. Cosmochim. Acta*, *59*, 661–677.

Nicolaus, M., C. Katlein, J. Maslanik, and S. Hendricks (2012), Changes in Arctic sea ice result in increasing light transmittance and absorption, *Geophys. Res. Lett.*, *39*, L24501, doi:10.1029/2012GL053738.

Nomura, D., H. Y. Inoue, and T. Toyota (2006), The effect of sea-ice growth on air–sea CO_2 flux in a tank experiment, *Tellus, Ser. B*, *58*, 418–426.

Nomura, D., T. Takatsuka, M. Ishikawa, T. Kawamura, K. Shirasawa, and H. Y. Inoue (2009), Transport of chemical components in sea ice and under-ice water during melting in the seasonally ice-covered Saroma-ko Lagoon, Hokkaido, Japan, *Estuarine Coastal Shelf Sci.*, *81*, 201–209.

Nomura, D., H. Y. Inoue, T. Toyota, and K. Shirasawa (2010a), Effects of snow, snowmelting and refreezing processes on air–sea-ice CO_2 flux, *J. Glaciol.*, *56*(196), 262–270.

Nomura, D., H. Eicken, R. Gradinger, and K. Shirasawa (2010b), Rapid physically driven inversion of the air-sea ice CO_2 flux in the seasonal landfast ice off Barrow, Alaska after onset of surface melt, *Cont. Shelf Res.*, *30*, 1998–2004.

Nomura, D., S. Koga, N. Kasamatsu, H. Shinagawa, D. Simizu, M. Wada, and M. Fukuchi (2012), Direct measurements of DMS flux from Antarctic fast sea ice to the atmosphere by a chamber technique, *J. Geophys. Res.*, *117*, C04011, doi:10.1029/2010JC006755.

Nomura, D., P. Assmy, G. Nehrke, M. A. Granskog, M. Fischer, G. S. Dieckmann, A. Fransson, Y. Hu, and B. Schnetger (2013), Characterization of ikaite ($CaCO_3 \cdot 6H_2O$) crystals in first-year Arctic sea ice north of Svalbard, *Ann. Glaciol.*, *54*(62), 125–131, doi:10.3189/2013AoG62A034.

Papadimitriou, S., D. N. Thomas, H. Kennedy, H. Kuosa, and G. S. Dieckmann (2009), Inorganic carbon removal and isotopic enrichment in Antarctic sea ice gap layers during early austral summer, *Mar. Ecol. Prog. Ser.*, *386*, 15–27.

Papadimitriou, S., H. Kennedy, L. Norman, D. P. Kennedy, G. S. Dieckmann, and D. N. Thomas (2012), The effect of biological activity, $CaCO_3$ mineral dynamics, and CO_2 degassing in the inorganic carbon cycle in sea ice in late winter-early spring in the Weddell Sea, Antarctica, *J. Geophys. Res.*, *117*, C08011, doi:10.1029/2012JC008058.

Papakyriakou, T., and L. Miller (2011), Springtime CO_2 exchange over seasonal sea ice in the Canadian Arctic Archipelago, *Ann. Glaciol.*, *52*(57), 215–224.

Parkinson, L. C., and D. J. Cavalieri (2012), Antarctic sea ice variability and trends, 1979–2010, *Cryosphere*, *6*, 871–880, doi:10.5194/tc-6-871-2012.

Parmentier, F. J. W., T. R. Christensen, L. L. Sørensen, S. Rysgaard, A. D. McGuire, P. A. Miller, and D. A. Walker (2013), The impact of lower sea-ice extent on Arctic greenhouse-gas exchange, *Nat. Clim. Change*, *3*, 195–202, doi:10.1038/nclimate1784.

Pringle, D. J., J. E. Miner, H. Eicken, and K. M. Golden (2009), Pore space percolation in sea ice single crystals, *J. Geophys. Res.*, *114*, C12017, doi:10.1029/2008JC005145.

Rysgaard, S., J. Bendtsen, B. Delille, G. S. Dieckmann, R. N. Glud, H. Kennedy, J. Mortensen, S. Papadimitriou, D. N. Thomas, and J.-L. Tison (2011), Sea ice contribution to air-sea CO_2 exchange in the Arctic and Southern Oceans, *Tellus, Ser. B*, *63*, 823–830.

Schindlbacher, A., S. Zechmeister-Boltenstern, G. Glatzel, and R. Jandl (2007), Winter soil respiration from an Austrian mountain forest, *Agric. Forest Meteorol.*, *146*, 205–215.

Screen, J. A., and I. Simmonds (2011), Declining summer snowfall in the Arctic: Causes, impacts and feedbacks, *Clim. Dyn.*, *38*, 2243–2256, doi:10.1007/s00382-011-1105-2.

Sejr, M. K., D. Krause-Jensen, S. Rysgaard, L. L. Sørensen, P. B. Christensen, and R. N. Glud (2011), Air–sea flux of CO_2 in arctic coastal waters influenced by glacial meltwater and sea ice, *Tellus, Ser. B*, *63*(5), 815–822.

Semiletov, I., A. Makshtas, S. Akasofu, and E. L. Andreas (2004), Atmospheric CO_2 balance: The role of Arctic sea ice, *Geophys. Res. Lett.*, *31*, L05121, doi:10.1029/2003GL017996.

Sommerfeld, R. A., R. C. Musselman, J. O. Reuss, and A. R. Mosier (1991), Preliminary measurements of CO_2 in melting snow, *Geophys. Res. Lett.*, *18*(7), 1225–1228.

Sommerfeld, R. A., A. R. Mosier, and R. C. Musselman (1993), CO_2, CH_4 and N_2O flux through a Wyoming snowpack and implications for global budgets, *Nature*, *361*(6408), 140–142.

Sommerfeld, R. A., W. J. Massman, R. C. Musselman, and A. R. Mosier (1996), Diffusional flux of CO_2 through snow: Spatial and temporal variability among Alpine–subalpine sites, *Global Biogeochem. Cycles*, *10*(3), 473–482.

Sun, X., and K. Matsumoto (2010), Effects of sea ice on atmospheric pCO_2: A revised view and implications for glacial and future climates, *J. Geophys. Res.*, *115*, G02015, doi:10.1029/2009JG001023.

Suzuki, S., S. Ishizuka, K. Kitamura, K. Yamanoi, and Y. Nakai (2006), Continuous estimation of winter carbon dioxide efflux from the snow surface in a deciduous broadleaf forest, *J. Geophys. Res.*, *111*, D17101, doi:10.1029/2005JD006595.

Takagi, K., M. Nomura, D. Ashiya, H. Takahashi, K. Sasa, Y. Fujinuma, H. Shibata, Y. Akibayashi, and T. Koike (2005), Dynamic carbon dioxide exchange through snowpack by wind-driven mass transfer in a conifer-broadleaf mixed forest in northernmost Japan, *Global Biogeochem. Cycles*, *19*, GB2012, doi:10.1029/2004GB002272.

Takahashi, T., et al. (2009), Climatological mean and decadal change in surface ocean pCO_2, and net sea-air CO_2 flux over the global oceans, *Deep Sea Res., Part II*, *56*, 554–577.

Thomas, D. N., S. Papadimitriou, and C. Michel (2010), Biogeochemistry of sea ice, in *Sea Ice*, 2nd ed., edited by D. N. Thomas, and G. S. Dieckmann, pp. 425–467, Wiley-Blackwell, Oxford.

Tison, J.-L., A. Worby, B. Delille, F. Brabant, S. Papadimitriou, D. Thomas, J. De Jong, D. Lannuzel, and C. Haas (2008), Temporal evolution of decaying summer first-year sea ice in the Western Weddell Sea, Antarctic, *Deep Sea Res., Part II*, *55*, 975–987, doi:10.1016/j.dsr2.2007.12.021.

Weiss, R. F. (1974), Carbon dioxide in water and seawater: The solubility of a non-ideal gas, *Mar. Chem.*, *2*, 203–215.

Winston, G. C., B. B. Stephens, E. T. Sundquest, J. P. Hardy, and R. E. Davis (1995), Seasonal variability in CO_2 transport though snow in a boreal forest, in *Biogeochemistry of Seasonally Snow-covered Catchments*, *228*, edited by K. A. Tonnessen, M. W. Williams and M. Tranter, pp. 61–70. The International Association of Hydrological Sciences Publ., Oxfordshire, U. K.

Yager, P. L., D. W. R. Wallace, K. M. Johnson, W. O. Smith Jr., P. J. Minnett, and J. W. Deming (1995), The northeast water polynya as an atmospheric CO_2 sink: A seasonal rectification hypothesis, *J. Geophys. Res.*, *100*(C3), 3289–4398, doi:10.1029/94JC01962.

Zemmelink, H. J., B. Delille, J. L. Tison, E. J. Hintsa, L. Houghton, and J. W. H. Dacey (2006), CO_2 deposition over the multi-year ice of the western Weddell Sea, *Geophys. Res. Lett.*, *33*, L13606, doi:10.1029/2006GL026320.

Zemmelink, H. J., J. W. H. Dacey, L. Houghton, E. J. Hintsa, and P. S. Liss (2008), Dimethylsulfide emissions over the multi-year ice of the western Weddell Sea, *Geophys. Res. Lett.*, *35*, L06603, doi:10.1029/2007GL031847.

Zhou, J., B. Delille, H. Eicken, M. Vancoppenolle, F. Brabant, G. Carnat, N.-X. Geilfus, T. Papakyriakou, B. Heinesch, and J. L. Tison (2013), Physical and biogeochemical properties in landfast sea ice (Barrow, Alaska): Insights on brine and gas dynamics across seasons, *J. Geophys. Res.*, *118*, 3172–3189, doi:10.1002/jgrc.20232.